On the relation between catalytic performance and microstructure of polycrystalline silver in the partial oxidation of methanol

H. Schubert, U. Tegtmeyer, D. Herein, X. Bao, M. Muhler and R. Schlögl

Fritz-Haber-Institut der Max-Planck-Gesellschaft, Faradayweg 4-6, D-14195 Berlin, Germany

Received 7 April 1995; accepted 25 April 1995

Electrolytic silver was investigated as partial oxidation catalyst for the conversion of methanol to formaldehyde. Using the mass spectrometric technique as on-line detector the relation between feed composition and temperature was determined allowing us to conclude that two simultaneous reaction pathways operate under steady state conditions. The microstructure was analysed by XRD and STM. A pronounced restructuring of the surface on the mesoscopic scale was detected. The atomic structure of the γ oxygen phase was determined on the (111) face of facets grown during reaction. The two reaction pathways find their counterparts in two distinctly different surface microstructures providing different geometries for the respective active sites. After prolonged time on stream the high surface mobility of the silver atoms removes all mesoscopic restructuring without changing the conversion characteristics. The observed restructuring is thus considered as a frozen large scale image of the continuously changing surface under reaction conditions.

Keywords: methanol oxidation; conversion to formaldehyde; silver; surface oxygen; STM; IMR-MS; adsorption-induced restructuring; atomic structure; texture; X-ray diffraction

1. Introduction

Early in the search for the mechanism of selective oxidation reactions catalysed by silver, it was found by XPS that at high temperature and high chemical potential of oxygen several distinctly differently bound oxygen species are present [1]. In our search for the mechanism of the selective oxidation of methanol to formaldehyde we described spectroscopic [2,3], structural [4,5] and mechanistic experiments [6] performed with polycrystalline catalysts under practical reaction conditions. In brief, we identified three species of atomic oxygen with distinct structural and energetic properties. A surface atomic species was termed according to its TDS behaviour as α form followed in energy of interaction by a bulk-dissolved

β species. A novel form of strongly interacting atomic oxygen with high local electron density was found to be incorporated into the top atomic surface layer and was termed γ oxygen. The corresponding structural model assumes a lattice expansion of 3% and a rotation of the top atomic layer by 2°. The resulting moiré pattern leads to a theoretical corrugation height of 0.053 nm.

The TDS data were correlated [6] with an instationary conversion experiment to the catalytic processes and the simultaneous operation of two different pathways of dehydrogenation and oxidehydrogenation was concluded. In this instationary experiment about 50% of the total conversion occurred rapidly with limited selectivity, whereas the other 50% were achieved with a long time constant but 100% selectivity to formaldehyde. The fast oxidehydrogenation reaction was attributed to surface oxygen (α and β), the slow reaction to a dehydrogenating centre associated with γ oxygen. These assignments are in agreement with earlier studies [7,8], which were lacking a detailed description of the oxygen species involved.

The catalytic activity coincides with massive morphological changes [9] driven by the structure sensitivity of the oxygen–silver interaction [4] and an adsorbate-induced high surface mobility of silver atoms at temperatures significantly below the melting point [10,11,5,4,12]. In order to find a relation between microstructural changes and catalytic performance we investigated electrolytic silver polycrystals by STM before and after they had been subjected to catalytic testing. Reference experiments with silver foils led to similar kinetic and morphological effects but allowed to apply textural analysis of the restructuring features which was used to check the statistical relevance of the images. In the literature we found two studies [13,14] of silver particles analysed with the STM before and after catalytic testing in search for microstructural effects.

2. Experimental

X-ray diffraction data were obtained from a silver foil treated in pure oxygen or in air at 923 K for 24 h. A Stoe Stadi P reflection instrument with Cu Kα radiation and a scintillation counter was used. Before and after each experiment the instrument was angle calibrated by a standard sample of silicon powder.

Electrolytic silver grains in particle sizes 0.2–0.5 mm were kindly provided by BASF. They were used in conversion experiments supported on a stainless steel grid in a quartz reactor as bed of 18 mm diameter and 10 mm height. A thermocouple sealed in quartz was used for temperature control of the air-jet heating system regulated by a PID system. This set-up enabled the rapid response of the energy input in order to keep the system isothermal. A feed system of three gas streams was combined in a preheated mixing zone immediately at the reactor inlet, which was operated downstream. A nitrogen stream was fed through the evaporator, which was fed by a methanol : water 40 : 60 mixture at an LHSV of 0.1 min^{-1}. A second stream was mixed from oxygen : nitrogen 20 : 80 with a flowrate selectable to a

wide range of stoichiometries. The stoichiometry factor is defined as the atomic ratio between methanol and oxygen multiplied by 100. A third gas stream of nitrogen was regulated such to maintain a total gas flow rate of 400 ml/min under all experimental conditions. The product gases were intensively cooled with a high-pressure water quartz cooler placed 20 mm downstream of the catalyst support mesh in order to suppress homogeneous decomposition of formaldehyde into CO and hydrogen.

The products were analysed in an Atomika IMR-MS 100 mass spectrometer using Kr for oxygen and Xe for all other gas components allowing such to quantitatively analyse the gas composition without peak overlaps with a time resolution of 6 s. Catalysts were preconditioned in reaction atmosphere for 2 days at 900 K before experiments were started. Steady states were reached well within 1 h after parameter changes.

The conversion experiments with feed compositions overstoichiometric in oxygen are dangerous as spontaneous explosions do occur. The on-line gas analysis showed that immediately prior to an explosion selectivity and conversion rose to 100% for CO_2. Rapid shut-off of the oxygen supply prevented the explosion to occur in most cases.

STM data were acquired from electrolytic silver particles and the silver foil before and after catalytic testing. Both tempering in air and transfer into UHV were detrimental for the structural resolution. Best results were obtained in dry oxygen atmosphere at ambient pressure. Mechanically prepared Pt–Ir tips were used in a Burleigh ARIS 6000 instrument. All data shown were acquired in the constant current mode with 200 mV gap voltage and 1 nA current setting. Scan speeds were 10–800 nm/s. Thermal drift required fast scan rates at high resolution (12 nm/s), secondary calibration (against Si 7 × 7 in UHV) of the instrument was done with oxidised HOPG in air.

3. Results

3.1. CONVERSION EXPERIMENTS

The main variables in the parameter space of the reaction in our reactor system are the temperature and the feed stoichiometry after setting catalyst load and total space velocity to values suitable for stable operation and on-line gas analysis. These conditions did not allow in our reactor to reach technical conversions [9] which can only be obtained at higher space velocities and catalyst loading. Fig. 1 shows the evolution of product yields at the optimum temperature as function of oxygen stoichiometry. The maximum yield is at understoichiometric feed compositions with respect to the oxygen content. This is a strong indication that oxidehydrogenation cannot be the only mechanism [15] involved under these reaction conditions. The selectivity to formaldehyde is limited at the oxygen-rich side due to increas-

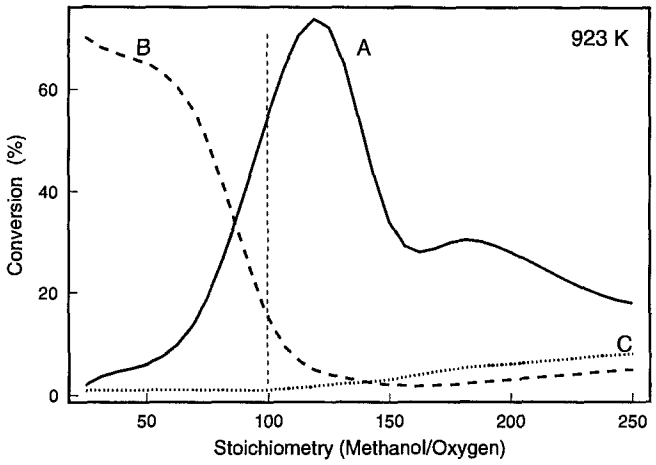

Fig. 1. Yield vs. composition diagram. (A) Formaldehyde, (B) carbon dioxide, (C) formic acid. The stoichiometry index is the atomic ratio methanol : oxygen (see Experimental).

ingly important total combustion and on the oxygen-lean side due to a reduction in total conversion. The oxygen-rich by-product formic acid occurs with notable selectivity only at the oxygen-lean side with a tendency of increasing selectivity for lower temperatures (maximum value at 723 K).

Fig. 2 shows temperature profiles at fixed feed stoichiometries. The data are clearly structured in three sections with temperature limits at 750 and at 850 K. In the low-temperature range we observe low conversions with a trend to higher values in oxygen-lean atmospheres. The central section between the two limits is almost invariant against compositional changes. In the high-temperature section

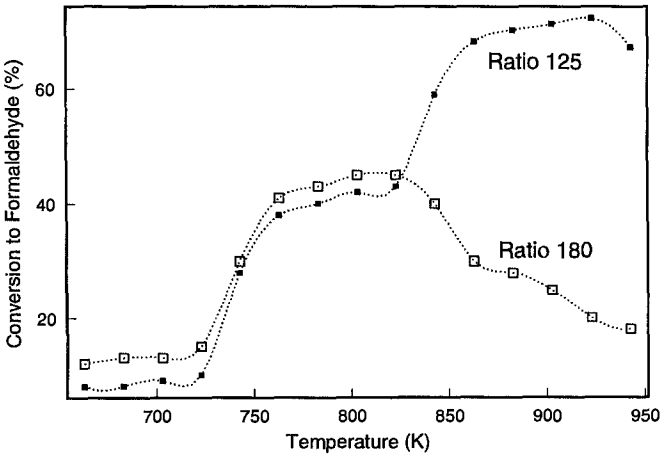

Fig. 2. Conversion to formaldehyde vs. temperature for two feed compositions close to stoichiometry (120) and rich in methanol (180).

the conversion depends strongly on the composition with the sharp maximum seen in fig. 1.

The data of both figures strongly imply the action of two independent reaction pathways with different requirements on oxygen partial pressures and activation energies. We concluded that also different microstructures should be present on the active catalyst surface. All microstructural studies were made with samples operated under the conditions of maximum formaldehyde selectivity.

3.2. TEXTURE

We analysed the powder X-ray diffraction patterns from the catalyst and from a reference silver foil. Both data sets fully agreed with each other but the reflection profiles from the catalyst were deformed as consequence of the coarse grain structure of the sample. The lattice constant of the pristine sample was found to be 408.6 pm, after oxidation in pure oxygen the constant was enlarged to 410.1 pm corresponding to 0.45% lattice expansion. This finding confirms the oxygen species analysis which found the β species to be dissolved in the silver bulk.

In fig. 3 drastic modifications are seen for the intensity distribution of the pat-

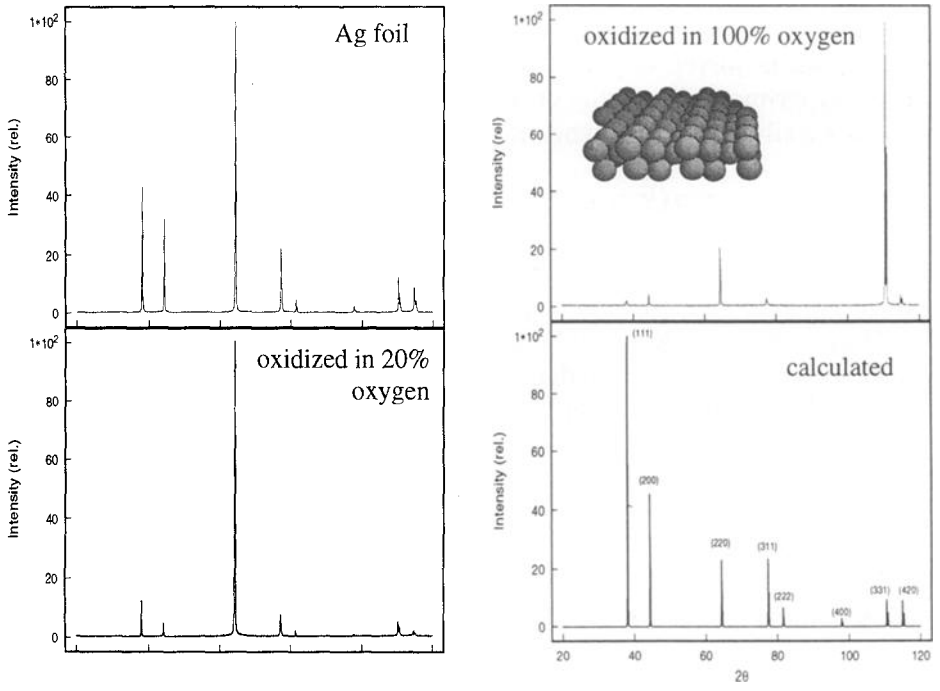

Fig. 3. X-ray diffraction wide scans for a silver foil as received, tempered in air and tempered in pure oxygen. The calculated intensity profile assumes statistical crystallite orientation and takes into account the corrections for the present scattering geometry (Bragg–Brentano).

tern from the foil relative to that from a statistical powder sample. The texture in (110) was induced by the rolling process of the foil. Tempering in air did not remove this texture but rather enhanced it into the same orientation (increase of the (220) reflection). Treatment in pure oxygen reverts the situation to a new texture expressed by a massive domination of the (331) reflection. Analysis with the Ω-scan technique revealed that the surface is (111) textured with a rough structure (excessive foots on the reflections) and an average misorientation of the rough features by 4.5° relative to the surface plane. The inset in fig. 3 illustrates that the (331) face is open and exposes the (111) orientation as double atomic row in its structure.

After exposure of the foil to reaction conditions at atmospheric pressure for 250 h the diffraction pattern showed still preferential orientation with both (331) and (220) intensities being strongly over-represented relative to the statistical (111) base peak.

These data show that on silver surfaces facetting occurs in (110) direction at low oxygen chemical potentials and into the (111) direction at high chemical potentials. In an earlier study [4] surface thermodynamics were shown to rationalize this effect. The relative change in oxygen chemical potential switching (110) facetting to (111) facetting is small compared to its difference between UHV experiments and ambient pressure studies.

The process involves no gas phase transport as we should have observed macroscopic transport of silver under the conditions of a strong downstream flow of inert gas which was, however, completely absent as long as oxygen was in the system. In control experiments involving only inert gases and methanol we observed rapid formation of a silver mirror downstream of the catalyst bed.

3.3. SURFACE MICROSTRUCTURE

Fig. 4 shows a typical silver surface prior to catalytic testing. The smooth appearance of such treated catalyst particles in an SEM [4] is resolved into an irregular hill-and-valley structure. The large-scale structure (one valley in fig. 4) has typical dimensions of 20–50 nm diameter and 5 nm height. On this structure a fine hill-and-valley structure is superimposed with dimensions of 5–20 nm diameter and 0.6–1.5 nm height. This microstructure is similar to that reported in the literature [16] for electrolytically roughened silver electrodes. It is dissimilar in dimensions to the hill-and-valley structure of electrodeposited silver on HOPG [17,18], of silver supported on SiC [13] and of silver foil exhibiting all even coarser structures and no fine structure on the hills. It can be concluded that electrolytically prepared silver is rich in structural defects which gave rise to highly uneven deposition conditions adding even more to the surface imperfection. Other forms of polycrystalline silver and of course single crystals exhibit much less surface imperfections [19,20] in the mesoscopic dimension.

Fig. 5 displays the surface microstructure of a conditioned catalyst after loading with oxygen at ambient pressure and exposure to methanol vapour at 10^{-6} mbar

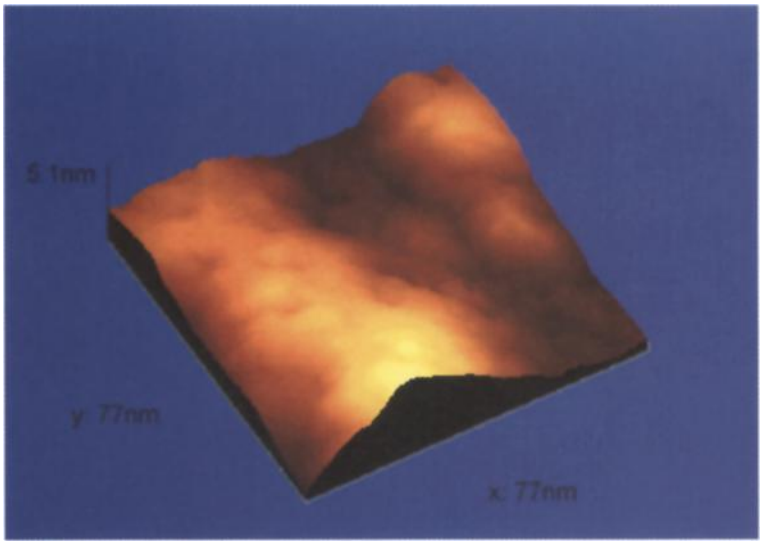

Fig. 4. STM image of an electrolytic silver particle before catalysis. The colour coding in the perspective view covers a height range from 0 (red) to 5.1 nm (yellow).

and 900 K. The line scan image indicates the dramatic change of the surface structure. Two facets with a terrace width of 400 nm and a step height of 40 nm form the coarse structure. The steps are smooth down to the atomic level (in enlargements, not shown). The terraces are rough exhibiting a furrow pattern with an average corrugation of 3 nm and distances of 20–40 nm. Their orientation is parallel to the large steps and no fine structure as on the untreated surfaces can be resolved.

The image illustrates the profound restructuring process arising from the conditioning of the catalyst. Oxygen exposure causes the facetting, whereas the low exposure to methanol removes the fine structure of the facets but not their disposition.

If the catalyst is then used under high pressure conditions the surface organisation as in fig. 5 remains detectable for up to 48 h on stream. Large smooth hills (20–60 nm diameter, up to 10 nm height) occurred with very sharp and regular boundaries. Such features have been described in the literature for thin films of silver immediately after their deposition [21–23].

After 300 h on stream all regular organisation has disappeared and a very smooth hill-and-valley structure prevails as can be seen from fig. 6. The sharp grain boundaries have disappeared as well as all finer structure. An exception are patches of small grains (diameter 2–3 nm, height 0.3–0.5 nm) which are mobile under the conditions of the tunnelling experiment. Their electrical conductivity seems to be much reduced compared to the support. We assign these objects to carbonaceous deposits arising from the extensive contact of the surface with organic material.

In order to investigate the surface microstructure prior to the modifications caused by the exposition to inert or reducing atmospheres we loaded the catalyst at

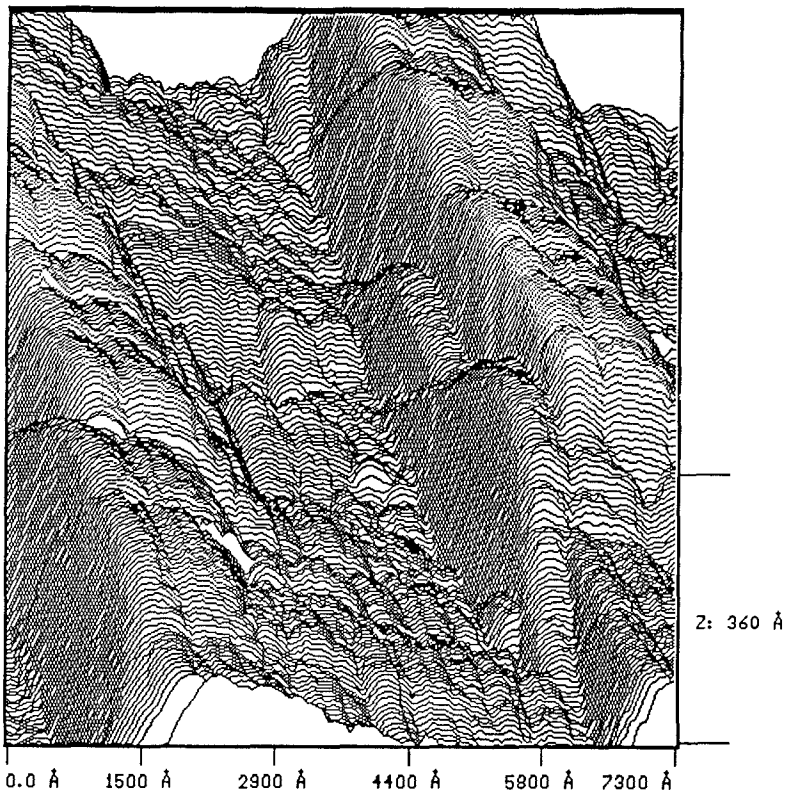

Fig. 5. STM image of an electrolytic silver particle after loading with oxygen and exposure to low pressures of methanol. The perspective view is presented as line scan image.

923 K with oxygen at 250 mbar to simulate practical reaction conditions. In fig. 7 the complete facetting of the whole surface can be seen. The dimensions of the facets are: height 7–25 nm and diameters from 40 to 160 nm with an average of 70 nm. These features exhibiting greater perfection in their shape are smaller than the facets seen in fig. 6. The facets on the foil all originated perpendicular to grain boundaries highlighting the relevance of surface imperfections as initiation centres for the restructuring.

The two sided of the facets were distinctly different in their microstructure. Fig. 8 compares the two patterns. One side was rough with a corrugation of 2 nm whereas the other side exhibited large terraces with mono- and diatomic steps characteristic of single crystal faces [5,19,20,24].

The large image in fig. 8 was obtained on a terrace from the flat side and exhibits finer features of atomic dimensions. A large superstructure discernible as low frequency component in the line scan with a unit cell size of ca. 7 nm and a corrugation of 0.02–0.04 nm is superimposed on an atomic structure of perfect hexagonal symmetry and a lattice parameter of ca. 0.5 nm detected as high frequency component in the line scan.

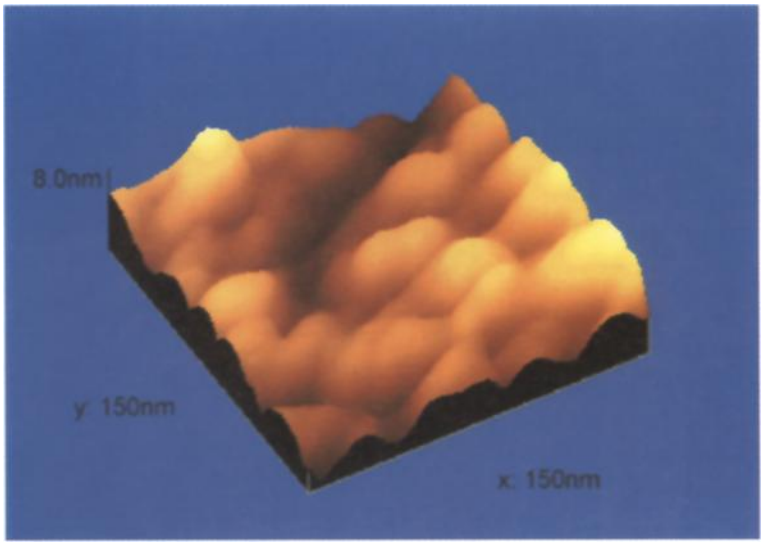

Fig. 6. STM image of an electrolytic silver particle after use in methanol oxidation for 300 h. The colour coding in the perspective view covers a height range from 0 (red) to 8.0 nm (yellow). The image may be compared to fig. 4.

The large superstructure was already observed with RHEED and described [5] as moiré pattern with a repeat of 6.9 nm and a corrugation of about 0.1 nm. The present images from the real catalyst are very similar to earlier STM images from

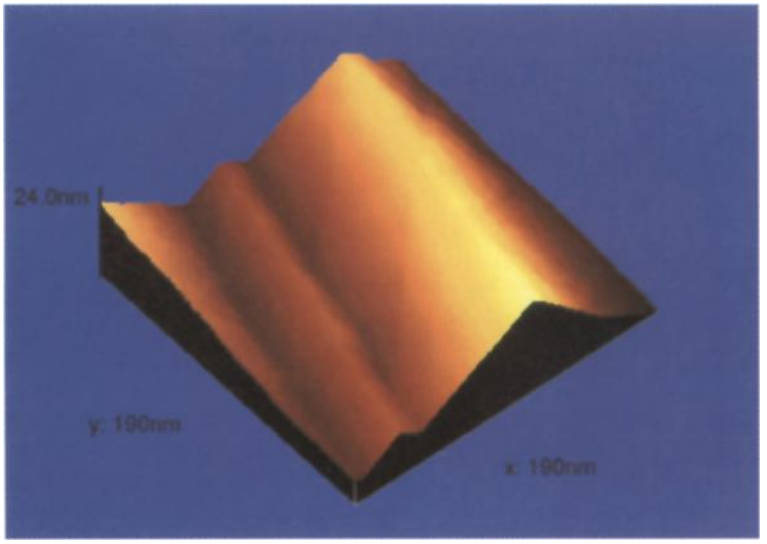

Fig. 7. STM image of an electrolytic silver particle after loading with oxygen. The colour coding in the perspective view covers a height range from 0 (red) to 24.0 nm (yellow). We note the different roughness on each face of the facet.

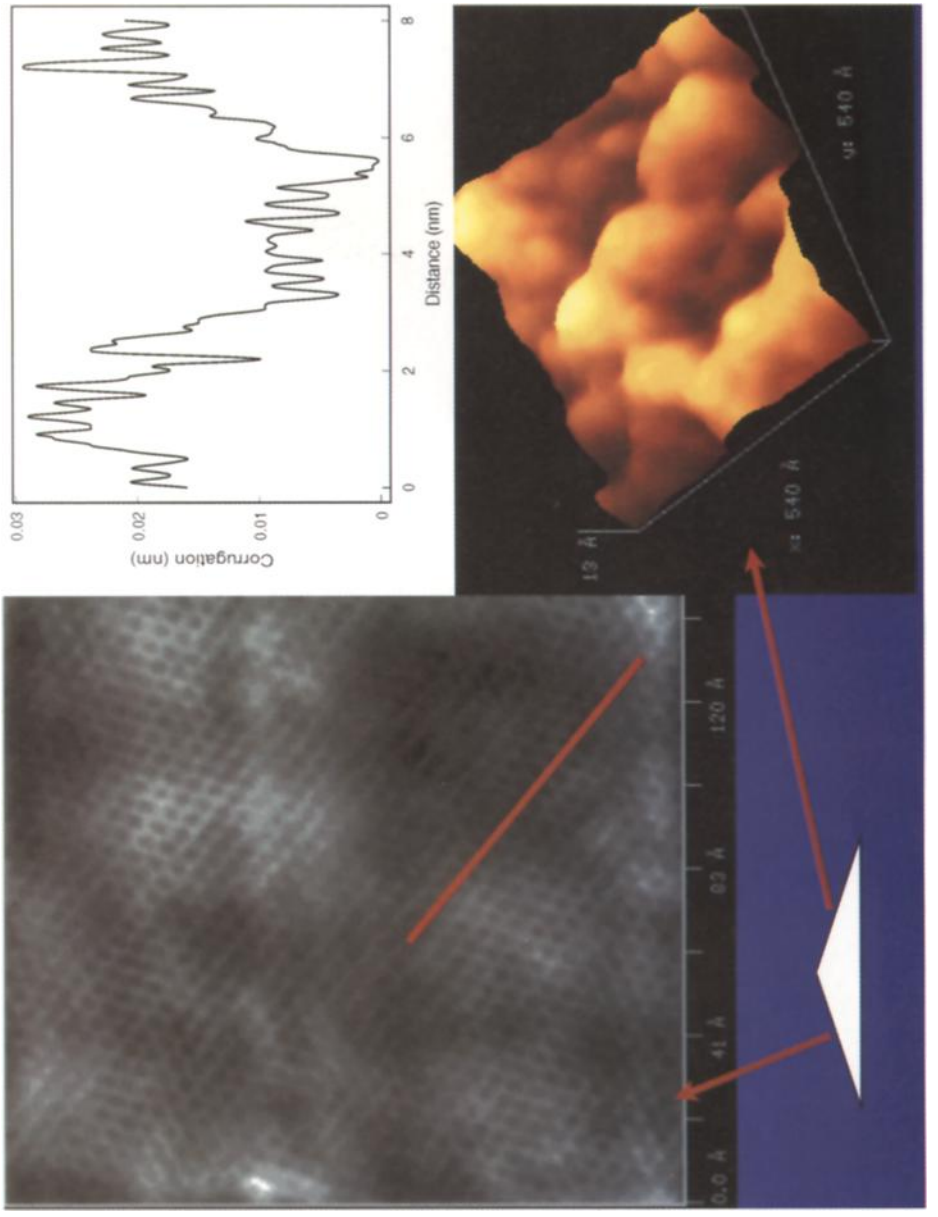

Fig. 8. STM images of a facet on an electrolytic silver particle after loading with oxygen. The schematic cross sectional drawing relates to a feature similar as seen in fig. 7. The large image is a top view representation (15 × 15 nm) of the (111) side. The height is coded as grey scale ranging from 0 (black) to 0.05 nm (white). The red line indicates the position of the line scan displayed in the top right side of the panel. The colour coding in the perspective view of the rough side of the facet covers a height range from 0 (red) to 1.3 nm (yellow).

an oxygen treated Ag(111) single crystal [5]. The present image from the catalyst exhibits, however, in contrast to the single crystal image a large number of irregularities and surface defects consistent with the different nature of the base materials.

The atomic structure was further resolved and can be seen in fig. 9. A hexagonal array of atoms is centred by a deep "hole". The interatomic distance of the light atoms is with 0.29 nm consistent with the Ag–Ag distance on Ag(111) of 0.285 nm. Also the corrugation amplitude of 0.02 nm is consistent with earlier literature reports [19,25]. The central holes with a distance of 0.53 nm are associated with intercalated oxygen atoms. Due to the image forming mechanism of STM the "contrast" is a superposition of topographic and local electronic structure [26]. It was found that the formation of γ oxygen is associated with a change in work function of 1.6 eV [2,27] which is large enough to account for the invisibility of the oxygen within the range of gap voltages which could be applied in oxygen atmosphere. The image represents thus a $\sqrt{3} \times \sqrt{3}$ R30 superstructure on Ag(111) caused by the incorporation of atomic oxygen. Such a superstructure has been observed before [28] and is consistent with the He scattering data [27] obtained from the γ oxygen phase.

Fig. 10 summarises the structural model for the γ oxygen phase as derived from the STM data. A central feature is the substitution of oxygen into the silver layer which is possible by the similar size of the atoms (silver atomic radius

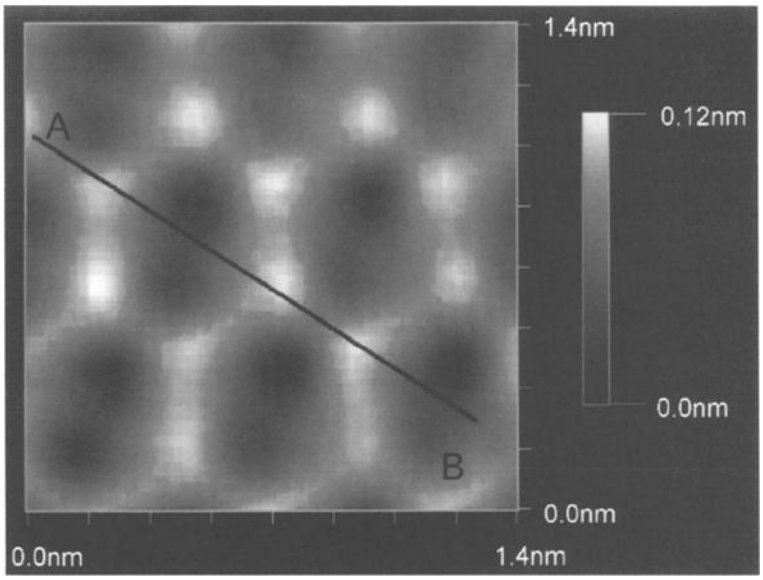

Fig. 9. Atomic resolution STM image of the (111) side of a facet of an electrolytic silver particle after loading with oxygen. The interatomic distance of the silver atoms (light maxima) measured along the line (A–B) is 0.29 nm. The very large corrugation height through the hexagon of 0.1 nm is a clear indication for the influence of local electronic effects and is no topographic property of the surface. For the same reason the silver atoms appear to be much too small relative to the central atom.

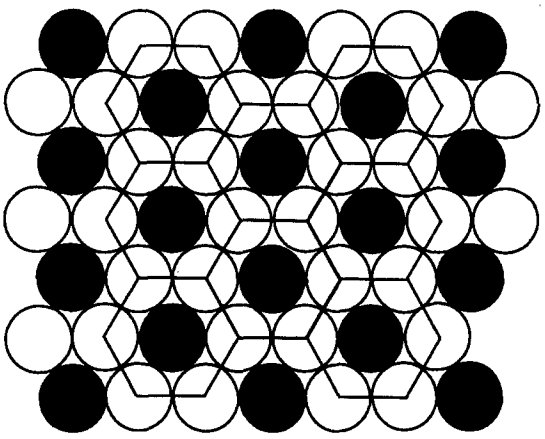

Fig. 10. Schematic representation of the atomic structure of γ oxygen (black) in the (111) face of silver (white). The metallic radius of silver with 1.44 nm allows to accommodate atomic oxygen with a small net negative charge (van der Waals radius 1.40 nm).

0.144 nm, oxygen atom van der Waals radius 0.140 nm). The composition of this unique oxygen structure is Ag_2O, well in agreement with earlier observations by electron spectroscopy [2]; the structural and electronic properties are, however, distinctly different from the bulk oxide [29]. This analysis confirms the statement that "oxygen incorporation is a facile process" [1] in silver at high temperatures and high oxygen chemical potential.

4. Discussion

The conversion data as direct "in situ" probe may be compared to the TDS data in the literature [6,16]. The three species of atomic oxygen can account for the three sections in the conversion/temperature profiles of fig. 2. The limit at 850 K corresponds to the beginning desorption of γ oxygen whereas the limit at 750 K marks the separation between the low-temperature α species and the segregation of the bulk-dissolved β species.

These assignments and the fact that above 750 K the CO_2 selectivity is low at all oxygen-lean stoichiometric ratios imply that the surface α species is responsible for the low-temperature conversion and the CO_2 production. The regimes of high and selective conversion fall within the ranges of existence of the bulk and subsurface species. As it is known [27] that β and γ oxygen do interconvert, it is not unambiguous to assign any of the two species to the two levels of high stable conversion. As the formation of γ oxygen requires a catalyst restructuring and exhibits the highest activation barrier, it seems plausible to associate the second plateau at oxygen-rich feeds to the efficient formation of the γ species.

This is in line with the microstructural observations revealing a more regular sur-

face structure at high oxygen partial pressures and the loss of detectable surface restructuring after exposure to pure methanol. In this context the detrimental abundance of oxygen (total oxidation) provides not only oxidation equivalents but also sufficient chemical potential for the surface restructuring required for the formation of the γ species with the beneficial side effect of suppressing the evaporation of the catalyst. The occurrence of the formaldehyde selectivity optimum at an "arbitrary" understoichiometric feed composition is also in line with this conjecture.

The conventional surface oxygen arising from gas phase adsorption or from segregation of the bulk-dissolved species is spectroscopically almost indistinguishable with respect to its origin. Kinetically, there seems to be a difference as the oxygen segregating from the bulk to the surface is more a selective dehydrogenation agent as the "hot" oxygen coming from direct dissociative gas phase chemisorption.

The reaction centres may be associated with the two sides of the facet structure. On the smooth side we see (111) faces reconstructed suitably to accommodate the γ oxygen structure which was clearly resolved by STM. The rough side provides suitable sites for surface oxygen and its equilibration with the bulk-dissolved species. In agreement with the RHEED and XRD experiments and earlier literature observations [10,11] we ascribe these rough sides to (100) and (110) faces.

The experiments show that it is mandatory to study the reaction system under conditions as close as possible to practical reaction conditions. In UHV the strong facetting and the generation of the γ oxygen phase cannot be observed. This has led earlier groups to the conclusion that the formaldehyde reaction occurs only via an oxidehydrogenation mechanism [15] neglecting the fact that in practical application [9] about 50% of the hydrogen balance occurs as dihydrogen. The recent report of a UHV oxygen-induced facetting of Ag(110) [12] is not in contradiction as the authors did not take into account the presence of the bulk-dissolved oxygen which they incorporated during crystal cleaning and which segregated during their low-pressure oxygen treatments. This analysis is also in line with other reports [30,31] of the absence of facets after high temperature-low pressure oxygen dosing.

The microstructural analysis has shown that under reaction conditions the catalyst restructures from an arbitrary state through a highly ordered faceted state into a new microscopically ill-defined state. It cannot be decided if this state is really amorphous or exhibits under reaction conditions the two sides of the facets in small patches. The XRD data together with the observation that the used catalyst is still preferentially oriented support the latter view. It can be excluded by the atomic resolution of the γ phase that experimental problems preclude the detection of atomic order on the extensively reacted catalyst. The fact that the surface is not structured in large single crystalline arrays under steady state conditions is well in agreement with the permanent and complete restructuring of all silver in the reaction zone. The processes of oxygen-induced re-crystallisation and reaction-induced atom mobility compete, with the surface dynamics winning over the crystallisation under stationary conversion conditions. The catalytic performance indicates the presence of γ oxygen even in the absence of mesoscopic restructuring and strongly

suggests the simultaneous presence of both types of microstructures. Their analytical characterisation became only possible as consequence of the catalyst isolation procedure allowing the respective surface microstructure to grow into dimensions suitable for STM observation.

Acknowledgement

This work was supported by the BASF and AG and the Bundesminister für Forschung and Technologie. We are grateful for intensive discussions to Drs. Dierks, Essig, Marosi, and for the co-operation to Dr. Krösche.

References

[1] E.L. Evans, J.M. Thomas, M. Barber and R.J.M. Griffith, Surf. Sci. 86 (1973) 245.
[2] C. Rehren, M. Muhler, X. Bao, R. Schlögl and G. Ertl, Z. Phys. Chem. 174 (1991) 11.
[3] X. Bao, B. Pettinger, G. Ertl and R. Schlögl, Ber. Bunsenges. Phys. Chem. 97 (1993) 322.
[4] X. Bao, G. Lehmpfuhl, G. Weinberg, R. Schlögl and G. Ertl, J. Chem. Soc. Faraday Trans. 88 (1992) 865.
[5] X. Bao, J.V. Barth, G. Lehmpfuhl, R. Schuster, Y. Uchida, R. Schlögl and G. Ertl, Surf. Sci. 284 (1993) 14.
[6] H. Schubert, T. Tegtmeyer and R. Schlögl, Catal. Lett. 22 (1993) 215.
[7] L. Lefferts, J.G. van Ommen and J.R.H. Ross, Appl. Catal. 23 (1986) 385.
[8] L. Lefferts, J.G. van Ommen and J.R.H. Ross, J. Chem. Soc. Faraday Trans. I 84 (1988) 1491.
[9] G. Reuss, W. Disteldorf, O. Grundler and A. Hilt, *Formaldehyde, Encyclopedia of Industrial Chemistry*, Vol. A11 (Verlag Chemie, Weinheim, 1988) pp. 619–651.
[10] A.J.W. Moore, Acta Metall. 6 (1958) 293.
[11] G.E. Rhead and H. Mykura, Acta Metall. 10 (1962) 843.
[12] J.S. Ozcomert, W.W. Pai, N.C. Bartelt and J.E. Reutt-Robey, Phys. Rev. Lett. 72 (1994) 258.
[13] P. Gallezot, S. Tretjak, Y. Christidis, G. Mattioda, A. Schouteeten, Y.-W. Chung and T.S. Sriram, Catal. Lett. 13 (1992) 305.
[14] C.N.R. Rao, H.K.N. Aiyer, T. Arunarkavalli and G.U. Kulkarni, Catal. Lett. 23 (1994) 37.
[15] M.A. Barteau and R.J. Madix, in: *The Chemical Physics of Solid Surf. and Heterogeneous Catalysis*, Vol. 4, eds. D.A. King and B.P. Woodruff (Elsevier, Amsterdam, 1982) pp. 95–142.
[16] I. Otsuka and T. Iwasaki, J. Vac. Sci. Technol. A 8 (1990) 530.
[17] L. Vazquez, A. Hernandez Creus, P. Carro, P. Ocon, P. Herrasti, C. Palacio, J.M. Vara, R.C. Salvarezza and A.J. Arvia, J. Phys. Chem. 96 (1992) 10454.
[18] R.S. Robinson, J. Vac. Sci. Technol. A 8 (1990) 511.
[19] T. Hashizume, M. Taniguchi, K. Motai, H. Lu, K. Tanaka and T. Sakurai, Surf. Sci. 266 (1992) 282.
[20] W. Obertenov, M. Höpfner, W.J. Lorenz, E. Budevski, G. Staikov and H. Siegenthaler, Surf. Sci. 271 (1992) 191.
[21] X.K. Zhao and J.H. Fendler, J. Phys. Chem. 94 (1990) 3384.
[22] E. Grantcharova and D. Dobrev, Cryst. Res. Technol. 28 (1993) 877.
[23] J.K. Gimzewski and A. Humbert, IBM J. Res. Develop. 30 (1986) 877.
[24] H. van Kempen and G.F.A. van de Walle, IBM J. Res. Develop. 30 (1986) 509.
[25] H.S. Kim, Y.C. Zheng and P.J. Bryant, J. Vac. Sci. Technol. A 8 (1990) 314.

[26] P.K. Hansma and J. Tersoff, J. Appl. Phys. 61 (1987) R1.
[27] X. Bao, M. Muhler, B. Pettinger, R. Schlögl and G. Ertl, Catal. Lett. 22 (1993) 215.
[28] K. Müller, Z. Phys. 195 (1966) 105.
[29] B. Pettinger, X. Bao, I. Wilcock, M. Muhler, R. Schlögl and G. Ertl, Angew. Chem. Int. Ed. Engl. 33 (1994) 85.
[30] W.L. Winterbottom, J. Appl. Phys. 40 (1969) 3810.
[31] W.L. Winterbottom, J. Appl. Phys. 40 (1969) 3803.